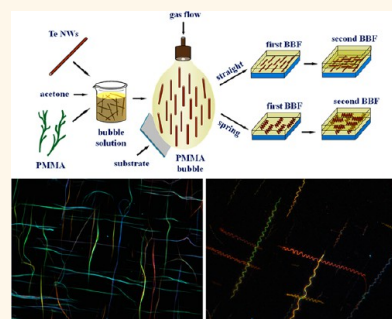


Soluble Polymer-Based, Blown Bubble Assembly of Single- and Double-Layer Nanowires with Shape Control

Shiting Wu,[†] Kai Huang,[‡] Enzheng Shi,[†] Wenjing Xu,[†] Ying Fang,[‡] Yanbing Yang,[§] and Anyuan Cao^{†,*}

[†]Department of Materials Science and Engineering, College of Engineering, Peking University, Beijing 100871, China, [‡]National Center for Nanoscience and Technology, Zhongguancun, Beijing 100190, China, and [§]College of Chemistry and Molecular Sciences, Wuhan University, Wuhan 430072, China

ABSTRACT We present here an efficient blown bubble method for large-scale assembly of semiconducting nanowires, with simultaneous control on the material shape. As-synthesized Te nanowires in powder form are dispersed in a polymethylmethacrylate (PMMA) solution, assembled in a large size bubble blown from the solution, and then transferred (repeatedly) to arbitrary substrates. By this way, we have obtained single-layer (aligned) and double-layer (crossed) Te nanowires as well as buckled Te nanosprings which are converted from initially straight nanowires *in situ* during bubble blowing. The PMMA bubble film can be removed by direct dissolution in acetone to expose nanostructures with clean surface while maintaining original configuration. After matrix removal, these clean nanowire and nanospring arrays can be fabricated into functional nanoelectronic devices such as photodetectors and gas sensors with high performance.



KEYWORDS: blown bubble films · nanowire assembly · nanosprings · double-layer cross-junctions

Integrated nanoelectronic and nanoelectromechanical systems based on semiconducting nanowires (NWs) or carbon nanotubes have potential applications in logical circuits, sensors and actuators, optical processing, and energy conversion.^{1–6} To fabricate function systems, nanomaterials must be assembled in large quantity with controlled orientation, distance, and even registration, which represent a bottleneck step from material synthesis to practical applications.⁷ Despite intensive efforts in this area, where many methods have been proposed such as the Langmuir–Blodgett technique and utilization of electrical/magnetic fields or liquid flow,^{8–17} large-scale and efficient assembly of powder from as-synthesized nanomaterials remains a demanding task. Recently, a nanoscale combing technique was adopted to assemble NWs with improved alignment and end registration, which was accomplished by prepatterned substrate regions with selective surface modification and exerting mechanical stress to slide and align NWs.¹⁸ Direct synthesis of horizontally aligned single-walled nanotube arrays provided an alternative way to fabricate

field-effect transistors with uniform properties.^{19–21} While most of the previous methods are applicable for straight shape nanostructures, assembly of other shape structures has been rarely explored. This is mainly because of several factors including the following: (1) it is difficult to precisely control the nanomaterial shape during mass production; (2) straight NWs or nanotubes are better aligned when they approach each other in some methods (*e.g.*, Langmuir–Blodgett),^{8–11} and (3) mechanical stress present during sliding/combing tends to straighten (curled) nanostructures.^{22,23}

In addition to the above work, our group has reported a blown bubble film (BBF) method to assemble nanostructures over large areas.^{24,25} Epoxy resin was used as the matrix polymer to disperse NWs or nanotubes and then blown into a bubble in which the fluid flow during bubble expansion generated shear stress to align nanostructures. Because those nanostructures were completely embedded within the epoxy matrix, reactive ion etching was carried out to etch away epoxy and expose nanostructures for making devices. Such drying etching process is an

* Address correspondence to anyuan@pku.edu.cn.

Received for review December 26, 2013 and accepted March 24, 2014.

Published online March 24, 2014
10.1021/nn406610d

© 2014 American Chemical Society

energy-intensive process, and the cured epoxy layer is hard to remove, which leads to inconvenience during subsequent device fabrication. Therefore, we have been searching for more environmentally benign polymers that can replace epoxy used in the BBF method. This polymer should be compatible for blowing bubbles and then removed by a simple way without influencing internal nanostructures.

Here, we show that a conventional polymer widely used in industry, polymethylmethacrylate (PMMA), can be used for the BBF method with several potential advantages over epoxy resin. We have achieved high density aligned semiconducting NWs, assembled in single or double layers, by blowing NW–PMMA bubbles. This is a general method for assembling various nanowires, and here we choose tellurium (Te) NWs as an example because they can be synthesized by a hydrothermal method in large quantity and also have useful optical and electronic properties. The PMMA matrix can be washed away by organic solvent, leaving clean NW arrays for fabricating high-performance nanoelectronic devices. Unprecedentedly, by controlling the bubble expansion process, straight NWs can be converted to regularly buckled nanosprings (NSs), offering a promising way to assemble nanostructures in large scale with controlled shape.

RESULTS AND DISCUSSION

The process of making PMMA-based BBFs is illustrated in Figure 1, which involves several steps. Double-layer configuration was obtained by repeated BBF transfer along perpendicular directions or at pre-defined angles. NS arrays were produced by allowing the bubble to shrink slightly before transferring to substrates. In this work, single-crystalline Te NWs with diameters of ~ 15 nm and lengths of ~ 50 μm were synthesized by a hydrothermal method in large yield (Supporting Information, Figure S1).²⁶ The NW powders were dispersed in acetone by magnetic stirring (ultrasonication was avoided which otherwise could shorten/break NWs rapidly), and the dispersion was further improved after adding PMMA at an appropriate concentration (see Experimental Methods for details). A homogeneous solution (as seen by eyes) was obtained which is critical for uniform NW assembly. The PMMA–acetone solution was blown into a single bubble by a small portable tool used for blowing soap bubbles, and the bubble was expanded upward along the long axis (which is the direction of aligned NWs) smoothly into an elongated cylinder with a diameter of 10–20 cm, which was sufficiently large for NW assembly (Figure 1b). Attaching the bubble to other substrates leads to smooth transfer of the bubble film onto a large piece of plastic sheet (Figure 1c), silicon wafer, or plastics in various geometries (Supporting Information, Figure S2). The NWs embedded within the polymer matrix can be directly observed in a dark-field

optical microscope, offering a convenient way to characterize their distribution and alignment. Optical images on a wafer-supported BBF reveal inside NWs that are well-aligned along the bubble expansion direction with a uniform and high density distribution across a $1.5 \times 2 \text{ cm}^2$ area (Figure 1d). The average distance between NWs is about $3.55 \pm 1.4 \mu\text{m}$, and the areal density is about $1.7 \times 10^5 \text{ cm}^{-2}$ with an angle deviation of $< 7^\circ$. Our BBF method is suitable for assembling individual (or bundled) NWs with controlled distance from several to tens of micrometers, which is favorable for device fabrication based on single or controlled number of NWs.

While PMMA was involved as the bubble matrix in our BBF process, it can be removed afterward by dissolution in acetone at room temperature. The key point here is to wash away PMMA without losing NWs or disturbing their alignment. To do this, we covered a second wafer on top of the PMMA BBF, and the two wafers were clamped by a magnet (Figure 2a). This setup was immersed in acetone for a period during which acetone gradually infiltrated into the gap between the two wafers and dissolved PMMA. The compressive force applied by the magnets could prevent NW movement during matrix dissolution and keep the NWs on the substrate after complete PMMA removal. Optical images of the embedded NWs in the BBF and exposed NWs after dissolving PMMA reveal that the original NW density and alignment can be well-maintained (Figure 2b,c). This solvent dissolution method also can be applied to NW arrays with a very high density, although some NWs appear relatively curled and the NW density has decreased slightly (Supporting Information, Figure S3). Since the PMMA matrix has been removed, the exposed NWs can be characterized by scanning electron microscopy (SEM). SEM images show very long aligned NWs anchored on a clean substrate (Figure 2d). In addition, we also transferred the BBF to a Si substrate with micro-trenches (300 nm deep and 30 μm wide) patterned by photolithography (Figure 2e) and obtained aligned NWs across the trenches (Figure 2f). We observe many NWs that contact the Si surface inside the trench with their ends suspended on the raised SiO_2 region, and these NWs are well-maintained after washing PMMA with acetone (Figure 2g). This result indicates that our BBFs may be transferred to nonplanar substrates with trenches or holes to obtain suspended nanostructures with potential applications as actuators.

Given that one bubble film consists of a single-layer of NWs, it is possible to tailor the NW density and create new configurations by multiple BBF transfer, as illustrated in Figure 3a. First, the areal density of NWs can be changed by layering BBFs sequentially along the same alignment direction. Optical images reveal that the number of NWs per area increases consistently after each bubble transfer, resulting in NW densities of 4.2×10^4 , 5.8×10^4 , and $9.1 \times 10^4 \text{ cm}^{-2}$ in one, two,

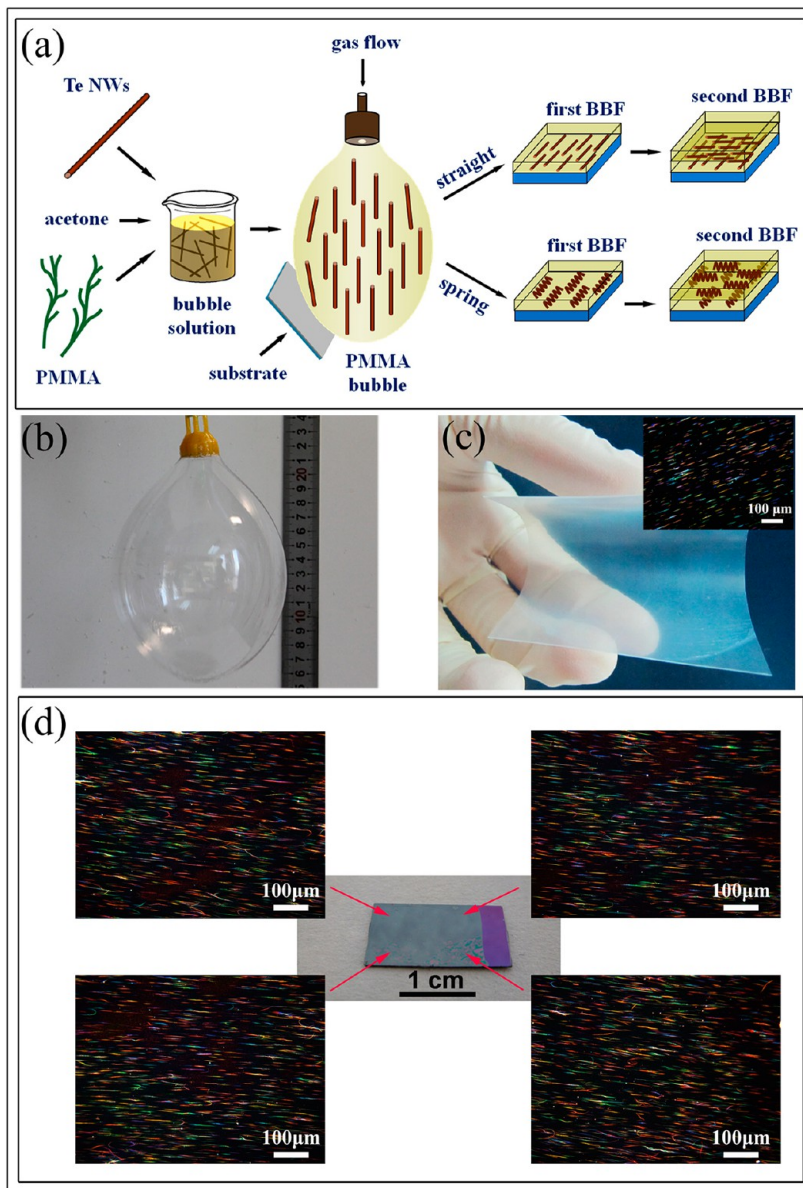


Figure 1. PMMA-based BBF assembly of Te NWs in various configurations. (a) Illustration of the BBF process in which a PMMA bubble containing assembled nanostructures is blown and transferred to substrates. Various configurations such as single- and double-layer NWs and NSS can be obtained. (b) Photo of a PMMA bubble which is about 15 cm in height and 9 cm in diameter. (c) Picture of a Te NW–BBF transferred to a rectangular 60 mm \times 80 mm plastic sheet. Inset: Dark-field optical image of the embedded Te NW arrays. (d) Photo of a Te NW-BBF transferred to a 15 mm \times 20 mm Si wafer. Four optical images show well-aligned and uniformly distributed Te NWs with a density of $1.7 \times 10^5 \text{ cm}^{-2}$ in different regions. The arrows point to the locations where images are recorded.

and three BBFs, respectively (Figure 3b–d). On the other hand, cross-junction structures were produced by layering BBFs along different directions. In this double-layer crossed configuration, the NW array aligned in one direction is placed on top of the first layer containing NWs along the perpendicular direction (Figure 3e,f). Typically, one NW would go across three to eight NWs perpendicularly depending on the NW length and average distance, forming a continuous two-dimensional network throughout the entire substrate. However, being embedded within the PMMA, NWs in the top and bottom layers are not touching each other initially. Removing PMMA by a similar

process described in Figure 2a leads to polymer-free, double-layer NWs at predefined orientations which come into direct contact (Figure 3g). The intersecting angle between NWs can be defined, as well, for example, 90° (Figure 3e–g) or 60° (Figure 3h–j). These double-layer networks are made from NWs orientated in two main directions (orthogonal or at a particular angle), which is different than the structure of other random networks. Furthermore, BBFs consisting of double-layer NWs can be transferred to transparent substrate (quartz) and exhibit high optical transmittance (>90%) (Supporting Information, Figure S4). With metallic NWs, multiple BBF stacking could result in

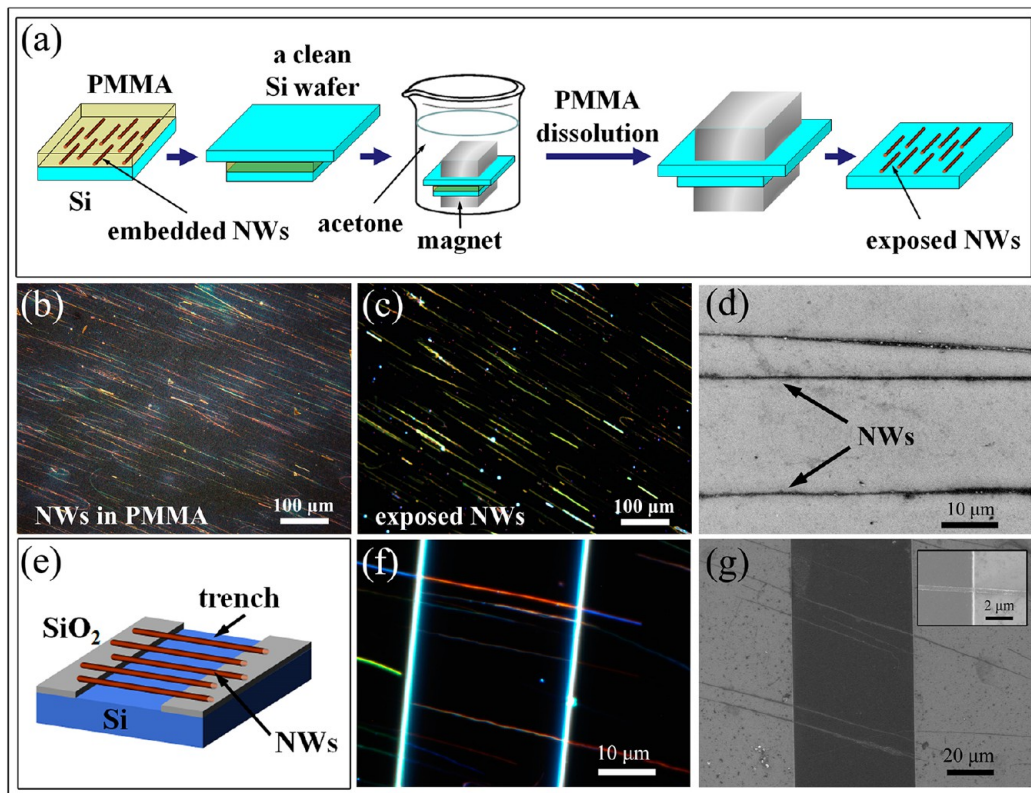


Figure 2. PMMA removal and NW exposure. (a) Illustration of the solution process in which the PMMA BBF is compressed between two Si wafers (clamped by magnet) and then washed away by acetone to expose NWs. (b) Optical image of the NW array embedded in the PMMA bubble film. (c) Optical image of the sample after removing PMMA, showing retained NWs with a similar density and high alignment. (d) SEM image of exposed, aligned NWs. (e) Illustration of assembled NWs suspended across a microtrench fabricated on a SiO₂/Si substrate. (f) Optical image of aligned NWs assembled on a 30 μm wide trench, and there are five NWs across the trench. (g) SEM image of suspended NWs after PMMA removal. Inset: End part of a NW suspended on the raised SiO₂ region.

conductive two-dimensional networks which may serve as transparent electrodes for thin film devices.

In addition to controlling the density and configuration of NW arrays, we can also change the straight NWs into wavy NSs *in situ* during BBF assembly (Figure 4a). We observe large-area aligned NSs distributed throughout the BBF, and each NS consists of regular buckles with wavelengths of 2–5 μm along the axis (Figure 4c,d). The mechanism for formation of such spring-like structures is under investigation; currently, we postulate that the interaction between the NWs and PMMA matrix may play a role in the NW shape change. Since initially the NWs were straight in the bubble solution, there must be some external factors that converted the NWs into NSs. During bubble expansion in air, the solvent (acetone) evaporated and the bubble film was dried slowly and shrunk slightly. The shrinkage of bubble film caused compressive force that consequently was applied to the embedded NWs (Figure 4b). The motion of NWs was limited by the surrounding PMMA matrix, and the NW had to buckle along the axis to accommodate the compressive stress/strain. A buckled NW spring contains many half-wavelength portions along the length; therefore, it is possible to use Euler's formula

to estimate the relationship between the compressive force (produced by bubble film drying) and the NW property (Young's modulus) through $F = (\pi^2 E I) / L^2$, where F is the critical force to initiate buckles, E is the NW modulus, I is the moment of inertia of a circular cross-section ($I = \pi d^4 / 64$, where d is NW diameter), and L is the half-wavelength. Therefore, L is determined by the two variables, F (compressive force generated during bubble shrinking) and E (NW modulus). There are several previous reports on buckled micro- and nanostructures (carbon nanotubes, Si nanoribbons, ZnO microwires, piezoelectric ribbons) which are produced by stretching and shrinking the plastic substrate, and the buckling mechanism has been analyzed based on the total energy in the system.^{27–32}

Interestingly, these NSs retain the buckled structure after PMMA removal, indicating a permanent deformation of NWs as the buckles cannot return to a straight shape. We therefore obtain clean, aligned NS arrays (without matrix) in which >95% NWs have been converted into NSs (Figure 4e). More complex structures such as double-layer crossed NSs have also been constructed by layering two BBFs with inside NSs aligned in perpendicular directions (Figure 4f). SEM characterization shows that the wavelengths of buckles vary at certain degree

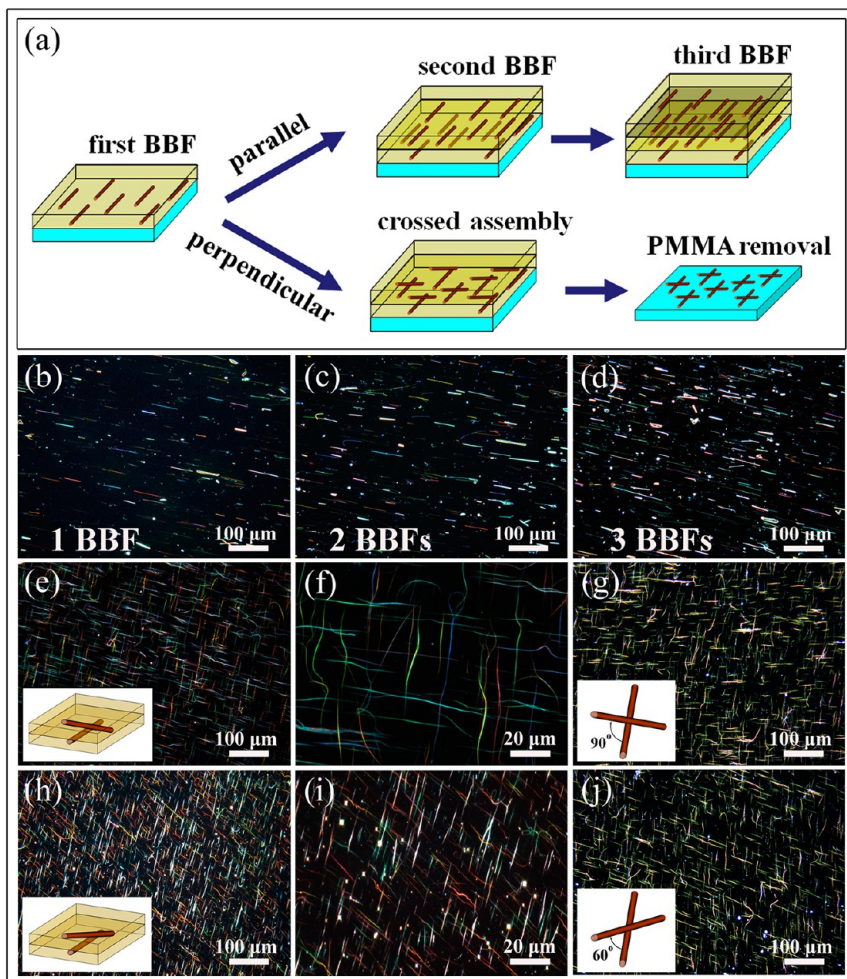


Figure 3. Layer-by-layer assembly of aligned and crossed NWs. (a) Illustration of the process in which multiple BBFs can be transferred sequentially to increase the NW density or create crossed junctions. (b–d) Optical images of the aligned NWs with increasing density in the first BBF and after the second and third BBF transfer. (e) Optical image of double-layer crossed NWs embedded in PMMA. Inset: Illustration of two perpendicular NWs in two BBFs (one in the top layer and one in bottom layer). (f) Enlarged view of (e). (g) Optical image of crossed NW arrays after PMMA removal. The intersecting angle of NWs remains at 90°. (h) Optical image of double-layer NWs embedded in PMMA and crossed at an angle of about 60°. Inset shows the configuration. (i) Enlarged view of (h). (j) Optical image of crossed NW arrays after PMMA removal. The intersecting angle remains unchanged.

along the axis direction, and also there is a wavelength fluctuation (typically $<10\text{ }\mu\text{m}$) between NSs (Figure 4g). Most of NS structures are often made by a bundle of individual nanowires that have been buckled collectively into the same shape (Figure 4h). The fluctuation of wavelength is caused by the different bundle diameters and perhaps the local variation of loading conditions through the bubble film. These NS arrays are potential candidates for constructing flexible stretchable nanoelectromechanical and energy-harvesting devices.^{27,29–31}

After the PMMA matrix is dissolved, the exposed clean Te NWs and NSs can be fabricated into functional devices by photolithography. Te NWs are a semiconducting material and have shown response to light and heat in previous studies.²⁶ We patterned long Au strips perpendicular to the aligned NWs as electrodes to define each device and measure the electrical properties (Figure 5a). Depending on the length of Au electrodes, the number of NWs connecting the

electrodes is different, and devices containing 7–33 NWs have been made accordingly. Optical and SEM images of selected devices and NWs within the channels are presented (Figure 5a,b), including one device consisting of 15 NSs (Figure 5c). Current–voltage (I – V) curve of a 33 NW device shows a resistance on the order of $0.5\text{ M}\Omega$, a dark current of $\sim 2.4\text{ }\mu\text{A}$, and a light current of $\sim 4.5\text{ }\mu\text{A}$ under 45 mW/cm^2 illumination (Figure 5d). Cyclic tests with a light on/off period of 4 min under 1 V bias show stable photoresponse upon illumination and reversible behavior for many cycles. We have measured devices with different number of NWs (or NSs) to compare their performance and found that the dark current flow (I_D) decreases with less number of NWs consistently, but the photoresponse can be clearly seen in all devices (Figure 5e). In particular, the light-to-dark current ratio (I_L/I_D) is stabilized in the range of 1.5–1.8, indicating a uniform behavior of NWs and NSs assembled by the BBF method (Figure 5f).

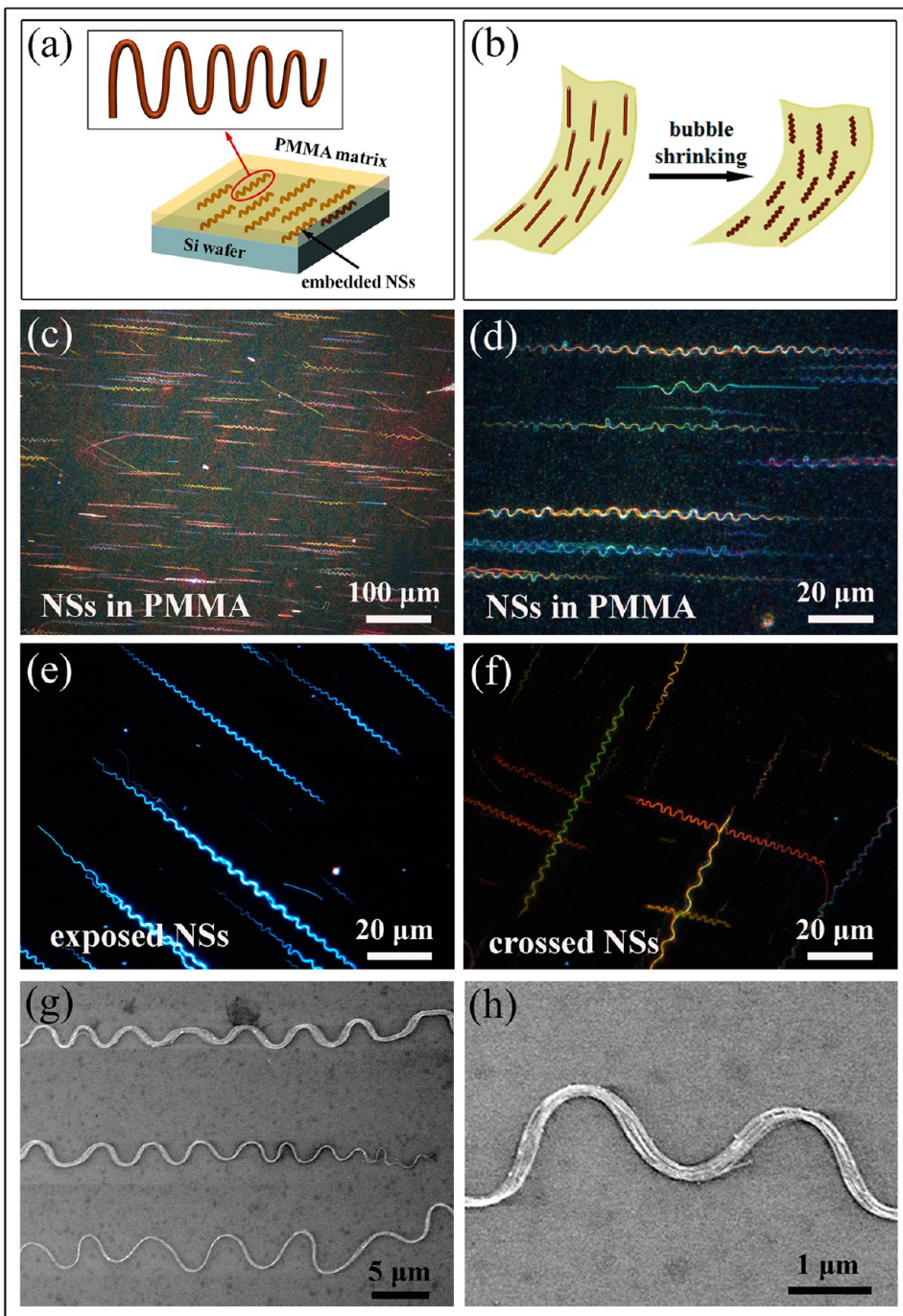


Figure 4. Assembly of aligned NSs. (a) Model of a NS array assembled in PMMA BBF. (b) Mechanism for the formation of NSs. Straight NWs are converted into NSs during the BBF assembly process due to bubble shrinking. (c,d) Optical images of aligned NSs embedded in PMMA. (e) Optical image of the exposed NS array. The spring shape is maintained after PMMA removal. (f) Optical image of crossed NSs in PMMA through a two-step assembly process. The intersecting angle is 90°. (g) SEM image of a NS array. (h) Enlarged view of a NS bundle.

A current ratio of $I_L/I_D = 1.6$ was reported in the literature based on thin films of Te TeNWs,²⁶ and here, a small number of aligned NWs also exhibit similar performance.

In addition, a gas sensor setup was built by enclosing a device with 19 Te NWs into a glass box, and diluted NO_2 in N_2 (0–1000 ppm) was introduced into the box while the I – V characteristics were monitored simultaneously (Figure 5g). Flowing NO_2 at different concentrations resulted in the change of I – V curves to

different slopes (resistances), indicating a reliable response of the Te NWs to NO_2 down to a concentration of 10 ppm (Figure 5h). High gas sensitivity observed here is attributed to the interaction between NO_2 and the lone-pair electrons from Te NWs.³³ The resistance of the NW array dropped rapidly at relatively low concentrations (10–100 ppm) and gradually stabilized. We also carried out the time domain measurements on a device consisting of a large number of Te NWs by

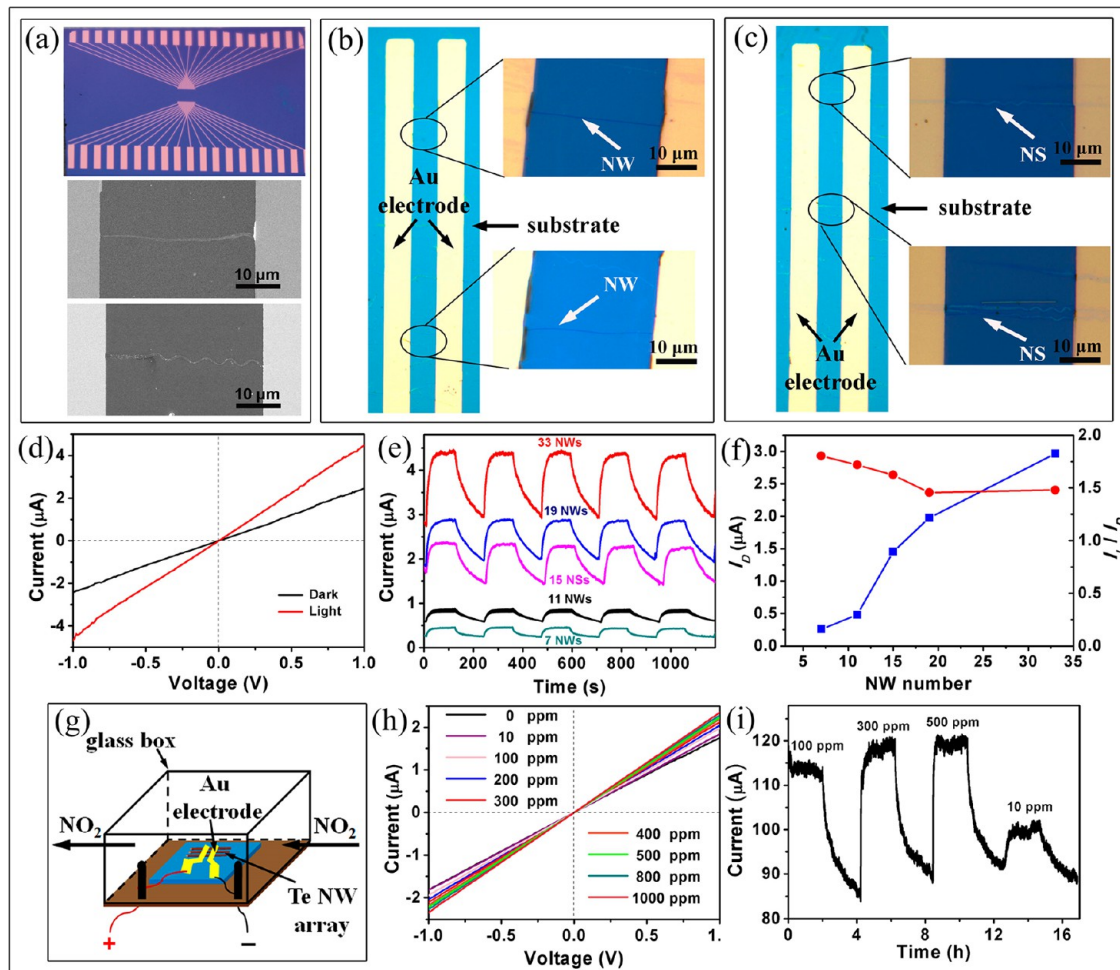


Figure 5. Electronic devices based on BBF-assembled Te NW/NS arrays. (a) Device configuration including patterned Au electrodes on SiO_2 and SEM images of single NW or NS connecting Au electrodes. (b) Optical images of a device based on aligned NWs, in which individual NWs within the channel are visible. (c) Optical images of a device based on aligned NSs. (d) I – V curves of a device containing 33 NWs measured in the dark and light. (e) Cyclic on–off photoresponse of a series of devices with different NW/NS numbers (from 7 to 33 NWs). (f) Dark current (I_D) values through devices with different NW numbers (blue curve) and the corresponding light-to-dark current ratios (I_L/I_D) (red curve). (g) Illustration of the gas sensor setup. A device with 19 Te NWs is enclosed in a glass box into which NO_2 at controlled concentrations is introduced. (h) Series of I – V curves recorded under different NO_2 concentrations up to 1000 ppm. (i) Time domain response for different NO_2 concentrations down to 10 ppm.

switching gas on and off every 2 h for cycles, which showed fast response when NO_2 was introduced, and reproducible adsorption/desorption behavior at NO_2 concentrations down to 10 ppm (Figure 5i). This property is useful for detecting toxic gases selectively from inertial atmosphere.

CONCLUSION

PMMA can be used for blown bubble assembly of nanostructures in a more environmentally benign way. The PMMA matrix can be dissolved by acetone to expose clean nanostructures for device fabrication.

With this method, many configurations can be fabricated such as aligned and crossed NW arrays and buckled NS arrays. In particular, large-scale formation of NSs (directly converted from straight NWs) offers a way to control the nanostructure shape *in situ* during assembly process. Te NWs assembled by the PMMA-based BBF show potential applications as photodetectors and gas sensors. Our bubble film method is suitable for large-scale assembly of different nanostructures and transfer to flexible substrates, and with better control on the nano-wire density, it is promising to fabricate diverse electronic and energy devices with improved performance.

EXPERIMENTAL METHODS

Synthesis of Te NWs. All chemicals are of analytical grade. We adopted a previous solution method²⁶ to synthesize Te NWs, with some modification on parameters. First, 1.0 g of

polyvinylpyrrolidone (PVP, $M_w \approx 40\,000$) and 0.1844 g of Na_2TeO_3 were mixed into 33 mL of distilled water. Then, 1.67 mL of hydrazine hydrate (85%, w/w%) and 3.33 mL of aqueous ammonia solution (25–28%, w/w%) were added.

The solution turned homogeneous after magnetic stirring for about 5 min. The solution was transferred to a 50 mL Teflon-lined stainless steel autoclave, closed, and maintained at 180 °C for 6 h. Finally, the autoclave was cooled to room temperature, and about 0.1 g of Te NWs was produced.

Characterization of Te NWs. First, we washed the Te NWs with acetone and centrifuged them at the rate of 4000 rpm/min for 4 min. The X-ray diffraction patterns were measured on Bruker D2 PHASER, and the sweep speed was 2°/min from 10 to 80°. Scanning electron microscope images were recorded on HITACHI S-4800. Transmission electron microscope (TEM) images, high-resolution TEM images, and selected area electron diffraction images were recorded on a Tecnai T20.

Preparation of Te NW–PMMA Bubble Solution. PMMA (9.6 g, $M_w \approx 996,000$) and 80 mL of acetone were mixed together under ultrasonication for 30 min with constant stirring. Then, ~0.2 g Te NWs dispersed in absolute ethyl alcohol (~5 mL) was added to the PMMA–acetone solution, which became homogeneous under magnetic stirring for 1 h. A small amount of a cationic surfactant, cetyl trimethylammonium bromide, was usually added for better dispersion of NWs.

Assembly of Te NW Arrays and PMMA Removal. A small portable tool with an air outlet of 12.5 mm diameter was used to blow bubbles manually. After the air outlet was dipped into the PMMA bubble solution, a thin membrane was formed on the outlet. By supplying a smooth air flow, a bubble was expanding upward and mainly along its long axis (this is the direction of aligned NWs). During the blowing process, the bubble tool was raised slowly to allow the bubble expansion to continue upward. This polymer bubble was like an elongated cylinder with 10–20 cm diameter and 15–20 cm height. Before the bubble film turned completely dry, a Si wafer (or other substrate) was placed close to the side bubble surface to let the bubble film cover the entire wafer gradually, to accomplish the transfer of PMMA BBFs containing assembled Te NWs. Double-layer BBFs were obtained through a two-step sequential transfer. The first BBF contained NW arrays aligned along one direction, and a second BBF was then layered on the top. The NW direction of the second BBF was controlled to be parallel or perpendicular to the first NW array, in order to obtain increased NW density or double-layer crossed configuration, respectively. Alternatively, we allowed the PMMA bubble to shrink slightly before its transfer to the Si wafer, in which case buckled NS (converted from straight NW) arrays can be produced. Parallel SiO₂ trenches (30 μm wide) were fabricated on a Si wafer with 300 nm oxide by photolithography. The NW and NS arrays were characterized under an Olympus BX51 M optical microscope.

To remove the PMMA matrix and obtain clean NWs or NSs, we covered a second wafer on top of the PMMA BBF and clamped the two wafers tightly by two magnets. This setup was immersed in acetone for up to 3 days to dissolve PMMA from the gap between the two clamped wafers.

Fabrication of Te NW-Based Electronic Devices. Te NW–BBFs were transferred to 20 mm × 15 mm Si wafers, and the PMMA matrix was removed by acetone. Then we coated a 1.5 μm layer of cured photoresist (S1813, Shipley) on top of the exposed Te NW arrays. Photolithography etching (MJB4, SUSS Micro Tec) and thermal evaporation (5 nm layer of Cr and 50 nm layer of Au) were carried out to deposit Cr/Au electrodes on Te NWs in predefined patterns using a mask. Electrical properties of the devices were measured at room temperature with the Probe Station 4 in. EB-4 and Keithley 2635A. Photoresponse was measured by illuminating the NW devices with a bulb (light intensity = 45 mW/cm²). Gas sensors were made by sealing a Si wafer with Te NW devices in a glass box. First, N₂ was flowed into the glass box at a concentration of 1000 ppm for 30 min to extrude air out. Then, NO₂ diluted in N₂ was introduced at different flowing rates to obtain different NO₂ concentrations (10–1000 ppm) within the box and surrounding the NW devices. For each concentration, the corresponding *I*–*V* curve was tested by a Keithley 2601 instrument after NO₂ was introduced for the same time (30 min). In addition, the time domain response data under different NO₂ concentrations was measured with a gas on/off period of 4 h under a constant bias

of 1 V, and in each period, NO₂ was first introduced for 2 h and then desorbed by N₂ flow for 2 h.

Conflict of Interest: The authors declare no competing financial interest.

Acknowledgment. This work was financially supported by the National Natural Science Foundation of China (Nos. 91127004 and 51325202). Y.F. acknowledges funding support by NSFC 21161120321.

Supporting Information Available: Structural characterization of as-synthesized Te NWs, transfer and characterization of PMMA bubble films to different substrates including plastics and quartz sheets. This material is available free of charge via the Internet at <http://pubs.acs.org>.

REFERENCES AND NOTES

- Takei, K.; Takahashi, T.; Ho, J. C.; Ko, H.; Gillies, A. G.; Leu, P. W.; Fearing, R. S.; Javey, A. Nanowire Active-Matrix Circuitry for Low-Voltage Macroscale Artificial Skin. *Nat. Mater.* **2010**, *9*, 821–826.
- Gao, P. X.; Song, J. H.; Liu, J.; Wang, Z. L. Nanowire Piezoelectric Nanogenerators on Plastic Substrates as Flexible Power Sources for Nanodevices. *Adv. Mater.* **2007**, *19*, 67–72.
- Takahashi, T.; Takei, K.; Adabi, E.; Fan, Z. Y.; Niknejad, A. M.; Javey, A. Parallel Array InAs Nanowire Transistors for Mechanically Bendable, Ultrahigh Frequency Electronics. *ACS Nano* **2010**, *4*, 5855–5860.
- Qi, Y.; Jafferis, N. T.; Lyons, K., Jr.; Lee, C. M.; Ahmad, H.; McAlpine, M. C. Piezoelectric Ribbons Printed onto Rubber for Flexible Energy Conversion. *Nano Lett.* **2010**, *10*, 524–528.
- Wang, X. F.; Xie, Z.; Huang, H. T.; Liu, Z.; Chen, D.; Shen, G. Z. Gas Sensors, Thermistor and Photodetector Based on ZnS Nanowires. *J. Mater. Chem.* **2012**, *22*, 6845–6850.
- Briseno, A. L.; Holcombe, T. W.; Boukai, A. I.; Garnett, E. C.; Shelton, S. W.; Frechet, J. J. M.; Yang, P. D. Oligo- and Polythiophene/ZnO Hybrid Nanowire Solar Cells. *Nano Lett.* **2010**, *10*, 334–340.
- Liu, X.; Long, Y.-Z.; Liao, L.; Duan, X. F.; Fan, Z. Y. Large-Scale Integration of Semiconductor Nanowires for High-Performance Flexible Electronics. *ACS Nano* **2012**, *6*, 1888–1900.
- Tao, A.; Kim, F.; Hess, C.; Goldberger, J.; He, R. R.; Sun, Y. G.; Xia, Y. N.; Yang, P. D. Langmuir–Blodgett Silver Nanowire Monolayers for Molecular Sensing Using Surface-Enhanced Raman Spectroscopy. *Nano Lett.* **2003**, *3*, 1229–1233.
- Whang, D.; Jin, S.; Wu, Y.; Lieber, C. M. Large-Scale Hierarchical Organization of Nanowire Arrays for Integrated Nanosystems. *Nano Lett.* **2003**, *3*, 1255–1259.
- Tao, A. R.; Huang, J. X.; Yang, P. D. Langmuir–Blodgett of Nanocrystals and Nanowires. *Acc. Chem. Res.* **2008**, *41*, 1662–1673.
- Mai, L. Q.; Gu, Y. H.; Han, C. H.; Hu, B.; Chen, W.; Zhang, P. C.; Xu, L.; Guo, W. L.; Dai, Y. Oriented Langmuir–Blodgett Assembly of VO₂ Nanowires. *Nano Lett.* **2009**, *9*, 826–830.
- Lee, M.; Im, J.; Lee, B. Y.; Myung, S.; Kang, J.; Huang, L.; Kwon, Y.-K.; Hong, S. Linker-Free Directed Assembly of High-Performance Integrated Devices Based on Nanotubes and Nanowires. *Nat. Nanotechnol.* **2006**, *1*, 66–71.
- Smith, P. A.; Nordquist, C. D.; Jackson, T. N.; Mayer, T. S.; Martin, B. R.; Mbindyo, J. Electric-Field Assisted Assembly and Alignment of Metallic Nanowires. *Appl. Phys. Lett.* **2000**, *77*, 1399–1401.
- Long, D. P.; Lazarcik, J. L.; Shashidhar, R. Magnetically Directed Self-Assembly of Carbon Nanotube Devices. *Adv. Mater.* **2004**, *16*, 814–819.
- Shekhar, S.; Stokes, P.; Khondaker, S. I. Ultrahigh Density Alignment of Carbon Nanotube Arrays by Dielectrophoresis. *ACS Nano* **2011**, *5*, 1739–1746.
- Shim, B. S.; Kotov, N. A. Single-Walled Carbon Nanotube Combing during Layer-by-Layer Assembly: From Random Adsorption to Aligned Composites. *Langmuir* **2005**, *21*, 9381–9385.

17. Huang, Y.; Duan, X. F.; Wei, Q. Q.; Lieber, C. M. Directed Assembly of One-Dimensional Nanostructures into Functional Networks. *Science* **2001**, *291*, 630–633.
18. Yao, J.; Yan, H.; Lieber, C. M. A Nanoscale Combing Technique for the Large-Scale Assembly of Highly Aligned Nanowires. *Nat. Nanotechnol.* **2013**, *8*, 329–335.
19. Kang, S. J.; Kocabas, C.; Ozel, T.; Shim, M.; Pimparkar, N.; Alam, M. A.; Rotkin, S. V.; Rogers, J. A. High-Performance Electronics Using Dense, Perfectly Aligned Arrays of Single-Walled Carbon Nanotubes. *Nat. Nanotechnol.* **2007**, *2*, 230–236.
20. Jin, Z.; Chu, H. B.; Wang, J. Y.; Hong, J. X.; Tan, W. C.; Li, Y. Ultralow Feeding Gas Flow Guiding Growth of Large-Scale Horizontally Aligned Single-Walled Carbon Nanotube Arrays. *Nano Lett.* **2007**, *7*, 2073–2079.
21. Jin, S. H.; Dunham, S. N.; Song, J. Z.; Xie, X.; Kim, J.-H.; Lu, C. F.; Islam, A.; Du, F.; Kim, J.; Felts, J.; et al. Using Nanoscale Thermocapillary Flows To Create Arrays of Purely Semiconducting Single-Walled Carbon Nanotubes. *Nat. Nanotechnol.* **2013**, *8*, 347–355.
22. Fan, Z. Y.; Ho, J. C.; Jacobson, Z. A.; Yerushalmi, R.; Alley, R. L.; Razavi, H.; Javey, A. Wafer-Scale Assembly of Highly Ordered Semiconductor Nanowire Arrays by Contact Printing. *Nano Lett.* **2008**, *8*, 20–25.
23. Yerushalmi, R.; Jacobson, Z. A.; Ho, J. C.; Fan, Z. Y.; Javey, A. Large Scale, Highly Ordered Assembly of Nanowire Parallel Arrays by Differential Roll Printing. *Appl. Phys. Lett.* **2007**, *91*, 203104.
24. Yu, G. H.; Cao, A. Y.; Lieber, C. M. Large-Area Blown Bubble Films of Aligned Nanowires and Carbon Nanotubes. *Nat. Nanotechnol.* **2007**, *2*, 372–377.
25. Yu, G. H.; Li, X. L.; Lieber, C. M.; Cao, A. Y. Nanomaterial-Incorporated Blown Bubble Films for Large-Area, Aligned Nanostructures. *J. Mater. Chem.* **2008**, *18*, 728–734.
26. Liu, J. W.; Zhu, J. H.; Zhang, C. L.; Yu, S. H. Mesostructured Assemblies of Ultrathin Superlong Tellurium Nanowires and Their Photoconductivity. *J. Am. Chem. Soc.* **2010**, *132*, 8945–8952.
27. Khang, D.-Y.; Jiang, H. Q.; Huang, Y.; Rogers, J. A. A Stretchable Form of Single-Crystal Silicon for High-Performance Electronics on Rubber Substrates. *Science* **2006**, *311*, 208–212.
28. Xiao, J.; Ryu, S. Y.; Huang, Y.; Hwang, K.-C.; Paik, U.; Rogers, J. A. Mechanics of Nanowire/Nanotube In-Surface Buckling on Elastomeric Substrates. *Nanotechnology* **2010**, *21*, 085708.
29. Lipomi, D. J.; Vosgueritchian, M.; Tee, B. C-K.; Hellstrom, S. L.; Lee, J. A.; Fox, C. H.; Bao, Z. N. Skin-like Pressure and Strain Sensors Based on Transparent Elastic Films of Carbon Nanotubes. *Nat. Nanotechnol.* **2011**, *6*, 988–979.
30. Rogers, J. A.; Someya, T.; Huang, Y. G. Materials and Mechanics for Stretchable Electronics. *Science* **2010**, *327*, 1603–1607.
31. Qi, Y.; Kim, J.; Nguyen, T. D.; Lisko, B.; Purohit, P. K.; McAlpine, M. C. Enhanced Piezoelectricity and Stretchability in Energy Harvesting Devices Fabricated from Buckled PZT Ribbons. *Nano Lett.* **2011**, *11*, 1331–1336.
32. Park, J. B.; Hong, W.-K.; Bae, T. S.; Sohn, J. I.; Cha, S. N.; Kim, J. M.; Yoon, J.; Lee, T. Strain Effects in a Single ZnO Microwire with Wavy Configurations. *Nanotechnology* **2013**, *24*, 455703.
33. Siciliano, T.; Filippo, E.; Genga, A.; Micocci, G.; Siciliano, M.; Tepore, A. Single-Crystalline Te Microtubes: Synthesis and NO₂ Gas Sensor Application. *Sens. Actuators, B* **2009**, *142*, 185–190.